A Mossbauer study of the nanocrystallization process in $Fe_{73.5}CuNb_3Si_{17.5}B_5$ alloy

1995 J. Phys.: Condens. Matter 7 4129

(http://iopscience.iop.org/0953-8984/7/21/012)

J. Phys : Condens. Matter 7 (1995) 4129–4143. Printed in the UK

A Mössbauer study of the nanocrystallization process in $Fe_{73.5}CuNb_3Si_{17.5}B_5$ alloy

T Pradell†, N Clavaguera‡, Jie Zhu§ and M T Clavaguera-Mora§

† ESAB, Universitat Politècnica de Catalunya, Urgell 187, 08036-Barcelona, Spain

‡ Física de l'Estat Sòlid, Departament ECM, Facultat de Física, Universitat de Barcelona, Diagonal 647, 08028-Barcelona, Spain

§ Grup de Física de Materials I, Departament de Física, Universitat Autònoma de Barcelona, 08193-Bellaterra, Spain

Received 23 January 1995

Abstract. The nanocrystallization process taking place during isothermal annealing at 490 °C in $Fe_{73.5}CuNb_3Si_{17.5}B_5$ amorphous alloy was studied as a function of annealing time by using transmission Mössbauer spectroscopy. Two different stages were found: a first one where mainly changes in the short-range order parameters of the amorphous phase occur, and a second one where nanocrystals with DO_3 structure appear. The silicon content in the nanocrystals decreases with annealing time to a final value of about 22 at.%. The first stage is also observed after 1 hour annealing at 450 °C or after cycling the amorphous sample from room temperature to 490 °C at a rate of 160 °C min^{-1} several times. The magnetic moments in the amorphous phase tend to align parallel to the surface of the ribbon especially in the first stage of nanocrystallization. The nanocrystalline phase formed in the second stage shows also a preferential magnetic orientation parallel to that surface. The existence of two stages is corroborated by differential scanning calorimetry, transmission electron microscopy and image analysis. The overall observations strongly suggest that nanocrystallization is driven by nucleation and growth.

1. Introduction

Since Yoshizawa *et al* [1] reported the excellent soft magnetic properties of the annealed Fe–Si–B-based amorphous alloy with some Cu and Nb called FINEMET, a lot of effort has been devoted to investigating the nanocrystalline structure responsible for those properties [1–6]. The nanocrystalline structure obtained during annealing of the amorphous alloy is linked to the presence of Cu and Nb. Since Cu is virtually insoluble in Fe, its local clustering enhances nucleation of the nanocrystalline grains [1–4]. The Nb addition stabilizes the residual amorphous phase and retards grain growth [1, 4–6].

The crystallization process of FINEMET materials has been studied by several techniques in order to obtain an overall view of the mechanisms that control the nanocrystallite formation [2–12]. However, the kinetics of the crystallization process is still not fully understood. Recently, several Mössbauer studies [7–9] have been performed to get deeper information about the crystalline and amorphous phases present in the onset of crystallization. General features are (i) an Fe–Si phase with DO_3 structure precipitates from the amorphous phase and (ii) there is a reduction of the average magnetic hyperfine field and an increase in the standard deviation of the magnetic hyperfine-field distribution of the remaining amorphous phase with respect to the initial one, a consequence of its enrichment in B, Nb, and Cu.

0953-8984/95/214129+15$19.50

The most widely studied material is $Fe_{73.5}CuNb_3Si_{13.5}B_9$. Rixecker *et al* [7] found that after one hour annealing at 550 °C the crystalline phase has about 18.6 at.% Si and the amorphous phase about 38.3 at.% Fe. Hampel *et al* [8] and Pundt *et al* [9] reported that after one hour annealing at 520 °C grains of about 10 nm size (about 20 at.% Si) and possibly Fe_2B and/or Fe_3B crystals in an amorphous phase with 50 at.% Fe were formed.

Miglierini [10] studied the onset of crystallization of amorphous $Fe_{73.5-x}CuNb_{3+x}Si_{13.5}B_9$ with $x = 0$ and 1.5 annealed at 550 °C. Nb addition reduces the average magnetic hyperfine field of the amorphous phase, increases the tendency of the magnetic moments to align parallel to the surface and slows down the Fe–Si nanocrystalline formation. The magnetic hyperfine-field distribution profile related to the amorphous phase is associated with two Fe neighbours sites: those rich in Si and B with a high magnetic field and those rich in Cu and Nb with a low magnetic hyperfine field.

Kataoka *et al* [11] studied the crystallization behaviour of $Fe_{74.5-x}Cu_xNb_3Si_{13.5}B_9$ alloys with $x = 0$, 0.5, 1.0, and 1.5. Without Cu they observed the simultaneous precipitation of BCC Fe–Si and Fe_3Si. When Cu was added the temperature of precipitation of Fe–Si phases is reduced. Magnetic moments of the amorphous and nanocrystalline phases align parallel to the surface of the ribbon.

Fujinami *et al* [12] studied $Fe_{73.5}CuNb_3Si_{16.5}B_6$ alloy and related compositions without Cu or/and Nb. They found that Cu and Nb have competing effects: Cu segregates at the very early stages of annealing, enhancing the Fe–Si formation; Nb inhibits Si and B diffusion retarding crystalline growth.

In this paper the kinetics of crystallization of an amorphous alloy $Fe_{73.5}CuNb_3Si_{17.5}B_5$ is presented. To have a detailed understanding of the nanocrystallization process transmission Mössbauer spectroscopy (TMS) and transmission electron microscopy (TEM) studies have been performed. Series of isothermal annealing at 490 °C and of heating and cooling cycles up to 490 °C have been designed. That temperature has been selected from previous differential scanning calorimetry (DSC) and X-ray diffraction (XRD) studies [13, 14].

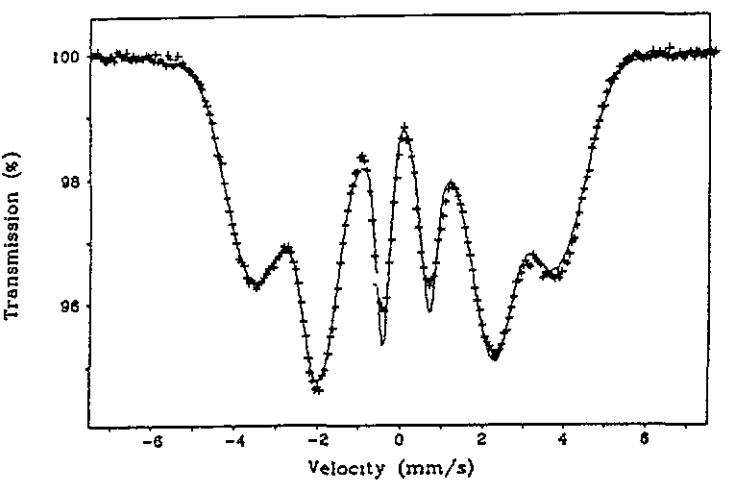

Figure 1. Mössbauer spectrum of the as-received amorphous alloy collected at room temperature. The fit is represented by a solid line.

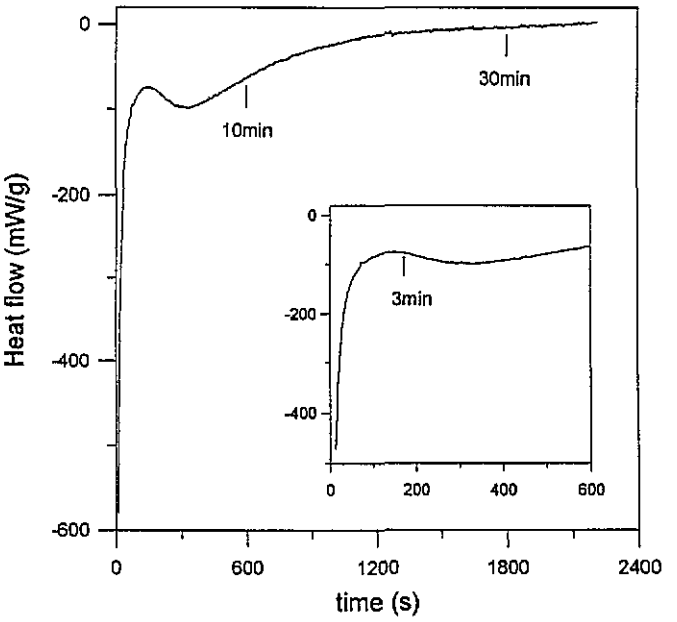

Figure 2. DSC isothermal curve at 490 °C. A crystallization peak can be observed between 3 and 30 min.

2. Experimental details

The $Fe_{73.5}CuNb_3Si_{17.5}B_5$ amorphous alloy was prepared by rapid solidification. The ribbons were 15 mm wide and 20 μm thick. The heat treatment of the samples and calorimetric experiments were carried out using a Perkin–Elmer DSC-7, which has a very precise control of the sample temperature. The specimens were heated in Au pans under purified Ar flow. Prior to each experiment, care was taken to remove the air from the DSC cell to avoid any oxidation of the sample.

TMS measurements at room temperature were performed on the as-received samples and on the heat-treated ones using a ^{57}Co in Rh source and calibrated with an α-Fe foil. The spectra were fitted with the program of Brand [15] by using a histogram magnetic hyperfine-field distribution and the Hesse–Rübartsch method [16], and including a linear correlation between the isomer shift and the magnetic field (DTI). This correlation is known to be responsible, together with the presence of anisotropic magnetic hyperfine fields, for the asymmetry in the spectrum of Fe–B-based amorphous alloys [17]. The spectra of the nanocrystalline samples have been fitted by superimposing sextets of Lorentzian lines corresponding to different Fe neighbourhoods in the Fe–Si phase, as it will be explained in more detail later, and with a Gaussian-shaped hyperfine-field distribution for the amorphous phase. A Gaussian distribution is a good compromise because of the lack of knowledge about the correct shape of the distribution for the amorphous phase. Moreover, it reduces the difficulty of the fitting procedure when amorphous and crystalline phases are simultaneously present. The magnetic hyperfine-field distribution in the amorphous phase has been fitted by superimposing 40 subspectra, from 0 T to 40 T with a step of 1 T, of 0.25 mm s^{-1} full width for each Lorentzian line, with a linear correlation between the isomer shift and the magnetic field.

TEM observations were done with a Hitachi H-800 operating at 200 kV. The grain size distribution of the nanocrystals was determined by image analysis of TEM microphotographs.

3. Results and discussion

3.1. Amorphous as-received sample

Mössbauer analysis of the as-received sample (figure 1) delivers a broad magnetic hyperfine-field distribution with an average magnetic field of about 20.9 T and a standard deviation of 5.15 T, characteristic for the Fe–B–Si-based amorphous alloys. The other parameters are given in table 1. The magnetic moments have a nearly random distribution as evident from the value, close to 2.0, of the ratio between the areas of the Mössbauer absorption lines 2 and 3 (A23 = 2.20).

Table 1. Mössbauer fitting parameters of the amorphous as received sample, the annealed sample at 177 °C and the annealed sample at 450 °C. Isomer shift relative to α-Fe (IS), change of isomer shift for each magnetic field (DTI), quadrupole splitting (QS), average magnetic hyperfine field (HF), standard deviation of the magnetic hyperfine-field distribution (STD) and area ratio between lines 2 and 3 (A23).

Sample	IS (mm s^{-1})	DTI (mm s^{-1})	QS (mm s^{-1})	HF (T)	STD (T)	A23
As received	0.008(5)	0.0055(3)	−0.015(3)	20.9(1)	5.15(13)	2.20(2)
177 °C	0.015(5)	0.0056(3)	−0.012(4)	21.00(7)	5.15(7)	2.64(3)
450 °C	−0.041(7)	0.0080(4)	0.018(3)	21.30(7)	5.10(8)	3.34(3)

3.2. Isothermal annealing at 490 °C*: ISO series*

Previous DSC measurements [13, 14] under isothermal annealing at 490 °C show a rapidly decaying exothermic signal overlapped with a crystallization peak, as reported in figure 2. The decaying exothermic signal lasts only a few minutes (3 min) while the crystallization peak extends from about 3 to 30 min. Moreover, the crystallization rate is slow enough for the study of the evolution of the sample under isothermal annealing. XRD shows that there is no iron boride formation even for long annealing time [14]. Further, under continuous heating the formation of borides occurs at temperatures higher than 700 °C [13]. For these reasons isothermal annealing at 490 °C for 3, 10, 30, 60, 120, and 240 min (ISO series) has been performed to study the nanocrystallization kinetics by TMS.

Two different crystalline structures are stable for an Fe–Si alloy: a BCC structure and a DO_3 ordered superstructure. Compositions with less than 10 at.% Si have a BCC structure with partial substitution of Fe by Si. In the contrast, DO_3 is defective but stable for compositions between 10 and 25 at.% Si [7, 18]. The BCC structure has a negligible probability for sites with less than 5 Fe near neighbours (five NN) and the values of the magnetic hyperfine fields related to the significant possible sites are 33.1 T (eight NN), 30.1 T (seven NN), 27.5 T (six NN). The DO_3 structure has two main sites: D and A. The D sites (all them having eight NN) have a magnetic hyperfine field of about 32.4 T. The A sites have magnetic hyperfine fields of 31–32 T (for eight NN and seven NN), 28.8 T (six NN), 24.5 T (five NN) and 19.8 T (four NN). The Mössbauer spectra of the ISO series have been fitted by superimposing one subspectrum for the amorphous and five subspectra corresponding to four, five, six, seven, and eight iron near-neighbour sites for the crystalline

phases. All of them are shown in figure 3. They are related to the possible existence of both BCC and DO_3 structures. The correlation of different iron near-neighbour sites with the relative areas of the crystalline subspectra is based on previous studies [18].

3.2.1. Amorphous phase evolution. The hyperfine parameters related to the amorphous phase in ISO series were deduced from the evaluation of the spectra obtained. They are presented in figure 4 and figure 5 which show, respectively, the changes of the IS (isomer shift) and QS (quadrupole splitting), and those of the HF (average magnetic hyperfine field) and STD (standard deviation of the magnetic hyperfine-field distribution). Two different stages are easily seen from the results presented in both figures. In the first stage IS and QS diminish, HF slightly increases and STD does not change significantly. This takes place in about the first three minutes of annealing time. In the second stage IS and QS increase, HF decreases, and STD increases. These two stages have the same duration as those found by DSC analysis.

The hyperfine parameters of the amorphous phase are related to the short-range order (SRO) of the iron near neighbours. Therefore, the slight but significant increase in the average magnetic hyperfine field during the first stage, together with the unchanged value of the width of the magnetic field distribution, should be assigned to an increasing magnetic interaction of the iron neighbour atoms. This increase in the magnetic interaction may be the result of two possible mechanisms. The first one is the diffusion out of the amorphous phase of elements which can shield the magnetic interaction among iron neighbours. Copper seems to be the most probable candidate because it is virtually insoluble in iron and its local clustering has already been observed [2, 3, 4]. The second one is a reduction of the free volume of the amorphous phase during relaxation. This effect has been reported [7, 9] after heating the sample at temperatures between 150 °C and 300 °C for long times (6 weeks). The changes observed in the SRO parameters (IS, QS, HF, and STD) support with both mechanisms.

During the second stage of crystallization, as shown in figure 5, the average magnetic hyperfine field decreases and the width of the magnetic field distribution increases dramatically. These changes correspond to a reduction of the magnetic interaction among iron neighbours due to the loss of iron (or the enrichment in Cu and Nb), consequent to the precipitation of the Fe–Si phase. Figure 6 shows the percentage of iron, which has been evaluated from the relative areas of the subspectra, in the amorphous phase and in the various sites of the nanocrystalline phase in the ISO series. In the first stage no big change in the iron content of the amorphous phase is detected. However, in the second stage the iron content decreases while nanocrystallization occurs. After four hours' annealing about 40 at.% Fe remains in the amorphous phase. Taking into account that the final composition of the nanocrystalline phase evaluated is $Fe_{78}Si_{22}$, the volume fraction of amorphous phase is about 42%. This result agrees with estimations made from the crystallization enthalpy measured by DSC [14].

Figure 7 shows the evolution of the area ratio of lines 2 and 3 (A23) observed for the amorphous phase during the isothermal treatment. In the first stage A23 clearly increases and reaches a value of about 3.35. Such a result, as also quoted by other authors [7–12], indicates a clear alignment of the magnetic moments parallel to the surface of the ribbon. In the second stage, the uncertainty in the evaluation of the A23 value is very high because of the presence of the subspectra corresponding to the nanocrystalline phase. However, considering the error bars shown in figure 7, it is steady or increases slightly.

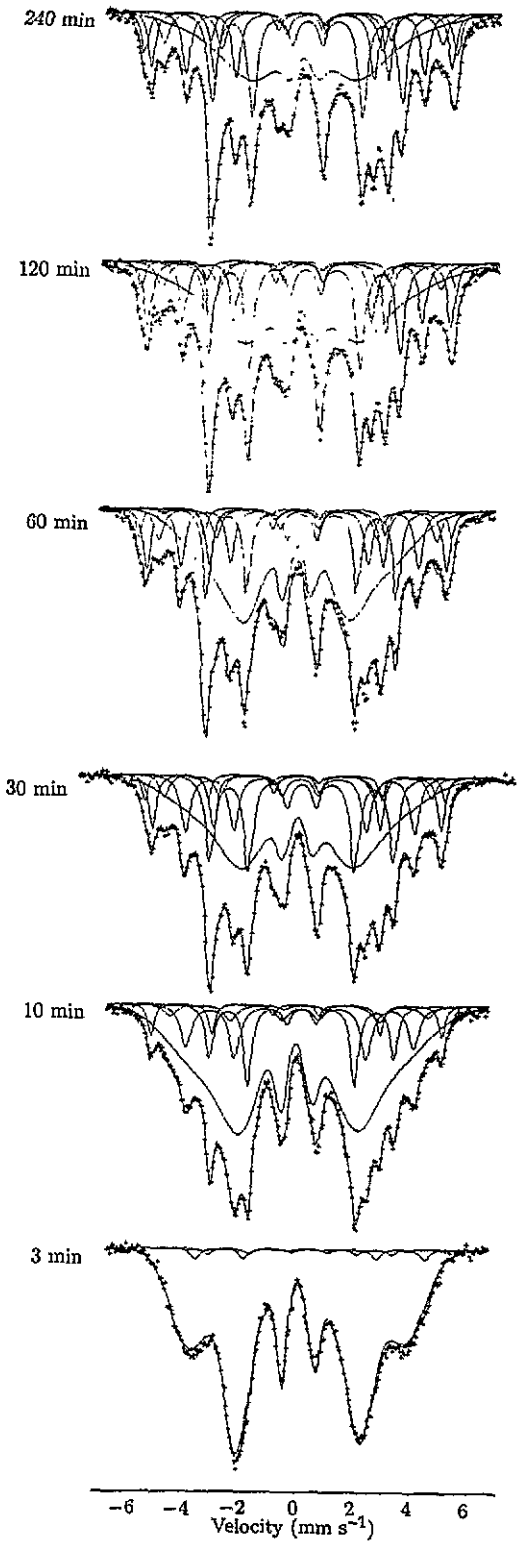

Figure 3. Mössbauer spectra corresponding to different annealing times of the ISO series. All the spectra are collected at room temperature. The fit and the fitted subspectra are represented as solid lines.

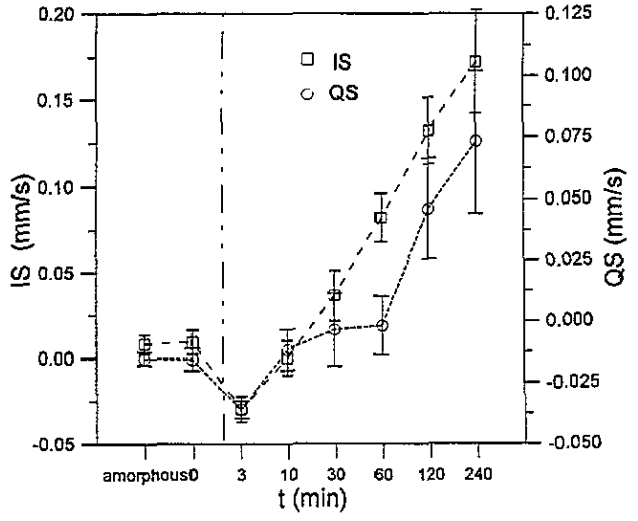

Figure 4. The isomer shift with respect to α-Fe (IS) and quadrupole splitting (QS) evolution as a function of annealing time in the ISO series.

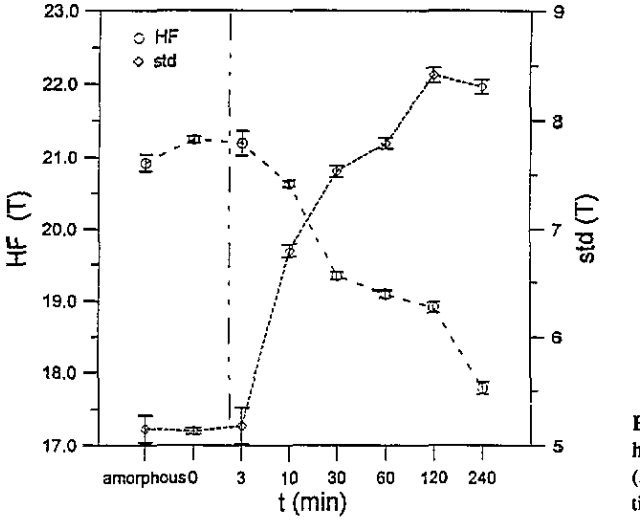

Figure 5. The average magnetic hyperfine-field (HF) and standard deviation (STD) evolution as a function of annealing time in the ISO series.

3.2.2. Nanocrystalline Fe–Si phase evolution. Figure 6 shows the percentages of iron content in the sites indicated as determined from the corresponding subspectra. From the significant presence of the four NN and five NN sites from the beginning of the crystallization process, it is inferred that the nanocrystals have a DO_3 structure. The values of IS, QS, and HF of each subspectrum appear unchanged during the whole crystallization process. Their average values and standard deviations are shown in table 2. The fitted values agree with those corresponding to a DO_3 Fe–Si phase.

The silicon content of the nanocrystalline phase was evaluated from the relative area between the sites four NN and (seven NN + eight NN) [7]. Presence of four NN and five NN in the first minutes' annealing indicates an structure with silicon content in the range of 22 to 25 at.% is formed. That is, the DO_3 nanocrystals form in an iron neighbourhood rich in silicon. After 30 minutes' annealing the DO_3 phase stabilizes to about 22 at.% Si. A silicon content in the nanocrystalline phase between 18 and 21 at.% has been reported [7–12]. That quantity depends on the original FINEMET composition. In our case the original Si content

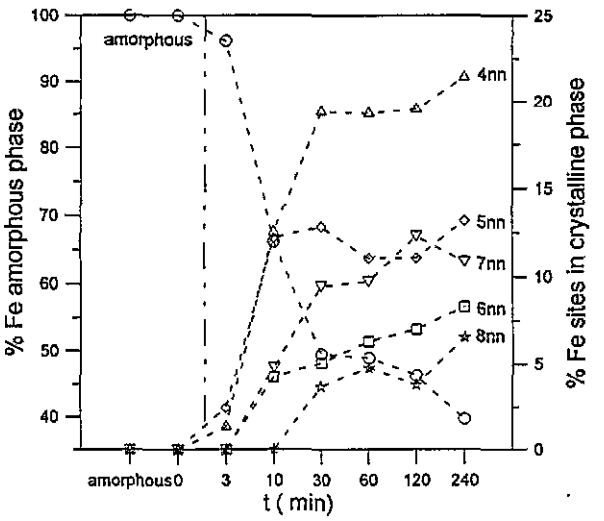

Figure 6. The percentage of iron in the amorphous phase and in the various sites of the nanocrystalline phase as a function of annealing time in the ISO series, determined from the relative areas of the Mössbauer subspectra.

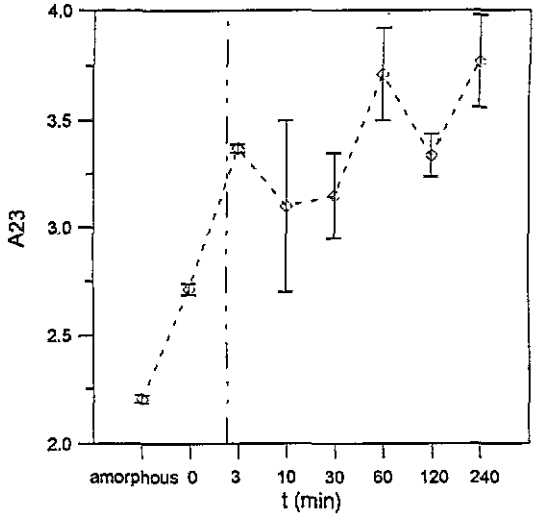

Figure 7. Area ratio of lines 2 and 3 (A23) evolution as a function of annealing time in the ISO series.

Table 2. Average values and standard deviation (between brackets) of the isomer shift relative to α-Fe (IS), quadrupole splitting (QS), and magnetic hyperfine field (HF) corresponding to the various subspectra related to the nanocrystals.

	IS ($mm\ s^{-1}$)	QS ($mm\ s^{-1}$)	HF (T)
Eight NN	0.026(7)	0.02(1)	32.4(1)
Seven NN	0.069(8)	0.01(1)	31.3(2)
Six NN	0.14(5)	−0.001(9)	28.8(5)
Five NN	0.190(6)	−0.001(1)	24.70(9)
Four NN	0.250(4)	0.008(9)	19.82(6)

is 17.5 at.%, higher than in other FINEMET materials. Therefore, a higher percentage of silicon in the nanocrystals would be expected. On the other hand, the high values of the relative areas of the six NN and seven NN subspectra might be related to the coexistence of BCC and DO_3 structures. Rixecker *et al* linked similar results to the possible sites in the

DO_3 structure [7] and other authors [9, 11] to the possible presence of Fe_2B and Fe_3B. No trace of iron borides was detected in our samples after four hours' annealing at 490 °C.

From the Mössbauer subspectra corresponding to the nanocrystalline phase a value of A23 close to 3.3 was found. This indicates a preferred orientation of the magnetic moments parallel to the surface of the ribbon.

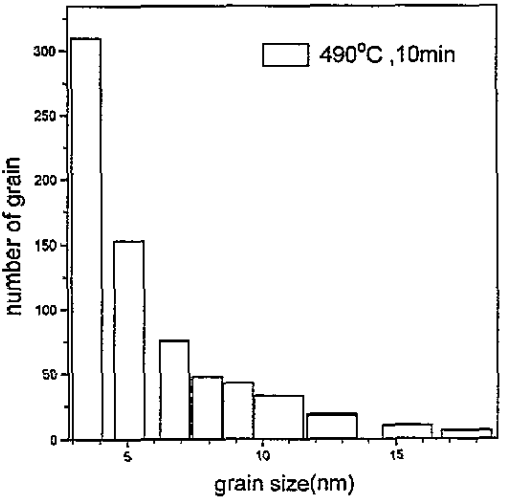

Figure 8. Grain size distribution of the sample annealed at 490 °C for 10 min determined by image analysis of TEM microphotographs.

Grain size analysis based on TEM images has ben performed. After three minutes' annealing the average grain size is $\langle d \rangle = 5$ nm with the standard deviation $\sigma = 5$ nm, and the biggest grain detected is $d_{max} \approx 10.5$ nm. After ten minutes' annealing the values quoted are $\langle d \rangle = 9$ nm, $\sigma = 5$ nm, $d_{max} \approx 20$ nm. After long annealing (four hours) they are $\langle d \rangle = 8.7$ nm, $\sigma = 10$ nm, $d_{max} \approx 27$ nm. The grain density increases dramatically from $N_v = (4.0 \pm 2.0) \times 10^{15}$ cm^{-3}, after three minutes' annealing, to $N_v = (2.5 \pm 1.0) \times 10^{16}$ cm^{-3}, after ten minutes' annealing. These results show that nanocrystals are mostly formed during the second stage of the crystallization process. Figure 8 shows the grain size distribution of the sample annealed for ten minutes. The exponential decrease of the grain density with increasing grain size indicates that no significant quenched-in nuclei growth occurs but there appears simultaneous nucleation and growth.

3.3. Detailed study of the first stage of crystallization: 0MS and 3MS

The main difficulty in studying the first stage of crystallization is the short timing involved. Therefore, two series of thermal treatments have been designed in order to get a better understanding of this first stage. The 0 min series (0MS) corresponds to heating and cooling cycles (once, twice, and four times) up to 490 °C. In the 3 min series (3MS) an isothermal heat treatment for three minutes at 490 °C is performed before cooling to room temperature, each time. Heating and cooling was carried out at 160 °C min^{-1} as well as in the ISO series.

The Mössbauer spectra obtained after performing the 0MS and 3MS series are shown in figure 9 and figure 10, respectively. Changes in the hyperfine parameters are shown in figure 11(a) and (b), figure 12(a) and (b). Comparing the changes of IS and QS shown in figure 11(a) with those shown in figure 4, it appears that the 0MS series has the same evolution as the ISO series in the first stage of crystallization; which is, IS and QS diminish. In contrast, the results presented in figure 11(b) for the 3MS series show such an evolution in the first heating cycle, but in the following heating cycles the IS and QS values increase,

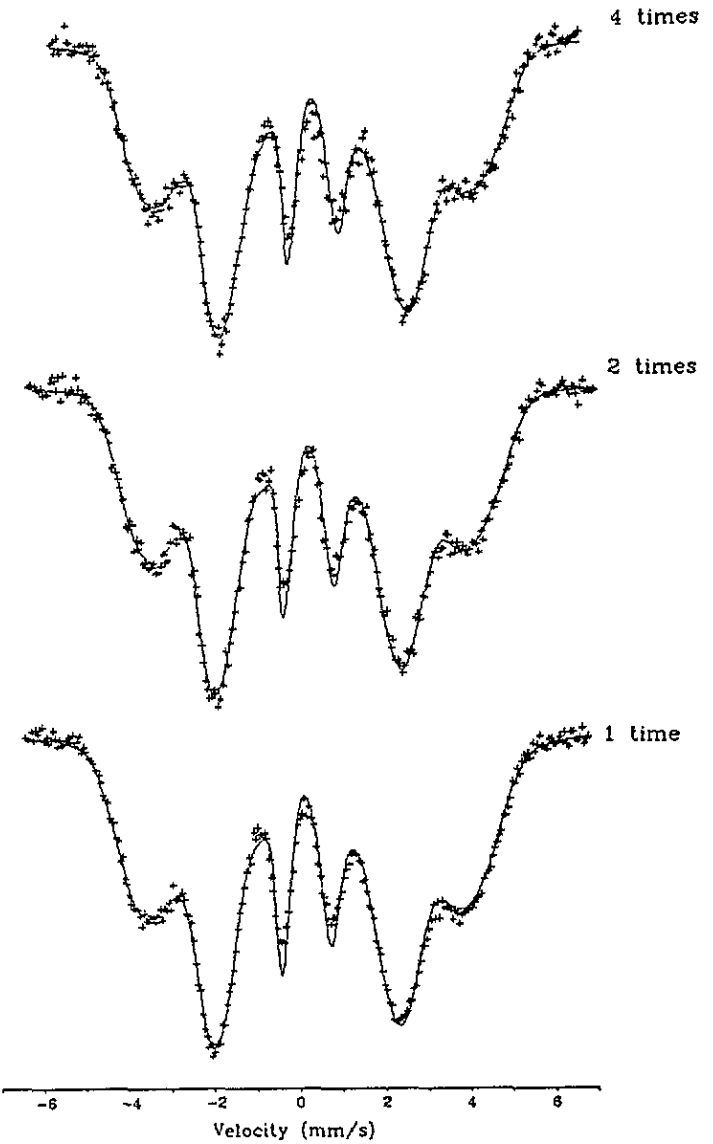

Figure 9. Mössbauer spectra corresponding to the 0MS series, corresponding to heating and cooling cycles (1 time, 2 times and 4 times) up to 490 °C.

as in the second-stage crystallization of the ISO series (see figure 4).

Figure 12(a) and (b) show the changes of HF and the STD for the 0MS and 3MS series, respectively. The 0MS series shows an increase in HF and no change in the STD value in the first heating cycle, as observed in the first stage of the ISO series (see figure 5). Subsequent heating cycles show an unchanged value or even slow reduction of the magnetic hyperfine field as in the second stage of the ISO series. The 3MS series data, presented in figure 12(b), shows the same evolution in the first heating cycle, but a reduction in the magnetic hyperfine field with an increasing standard deviation after twice annealing, as in the second stage of the ISO series.

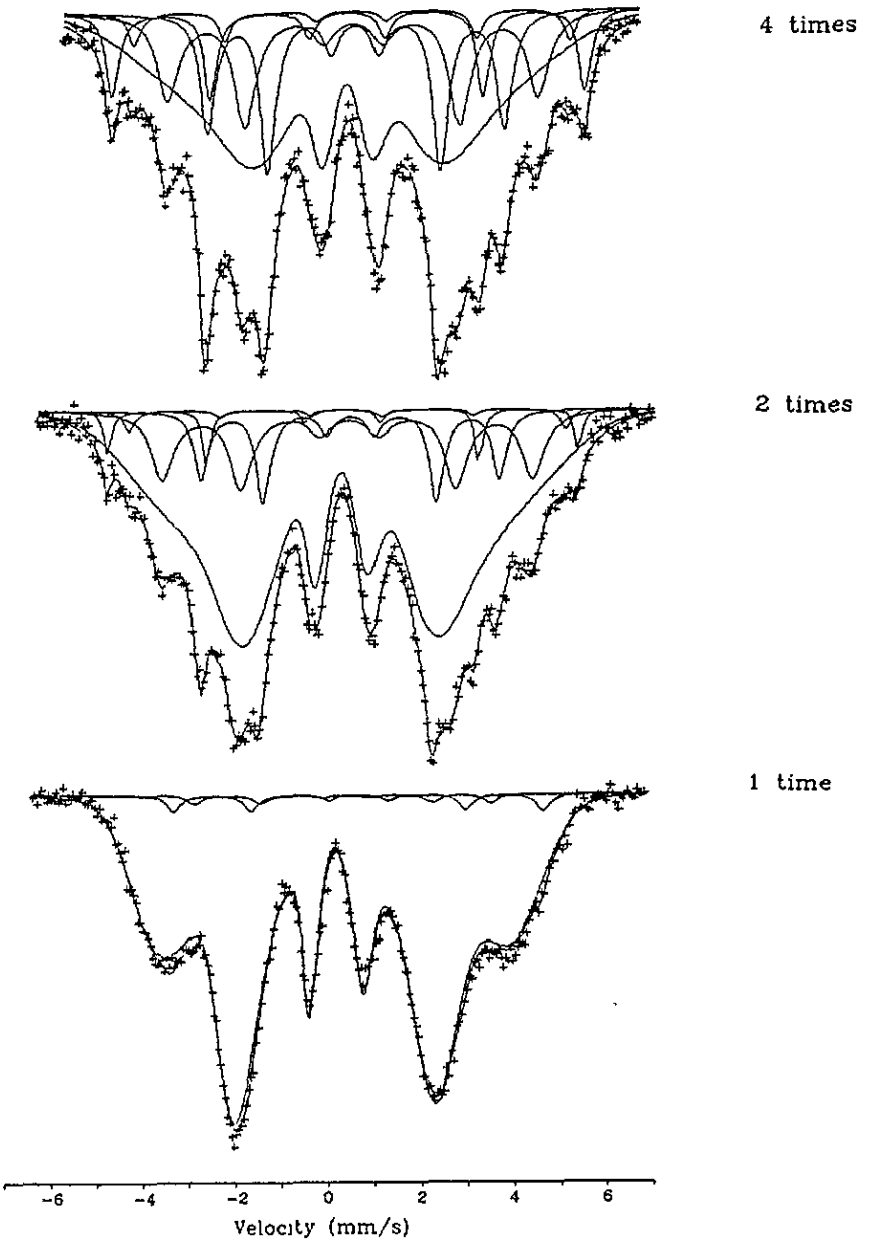

Figure 10. Mössbauer spectra corresponding to the 3MS series, cycles of three minutes' isothermal annealing at 490 °C before cooling to room temperature (1 time, 2 times and 4 times).

Figure 13 shows the percentage of iron in the amorphous matrix and in the various iron near-neighbour sites of the nanocrystals formed in the 3MS series. The evolution of all these quantities is very similar to that obtained after ten minutes' annealing in the ISO series.

Therefore, it can be concluded that during subsequent heating and cooling cycles the nanocrystallization process develops in the same way as during isothermal annealing: (i) SRO

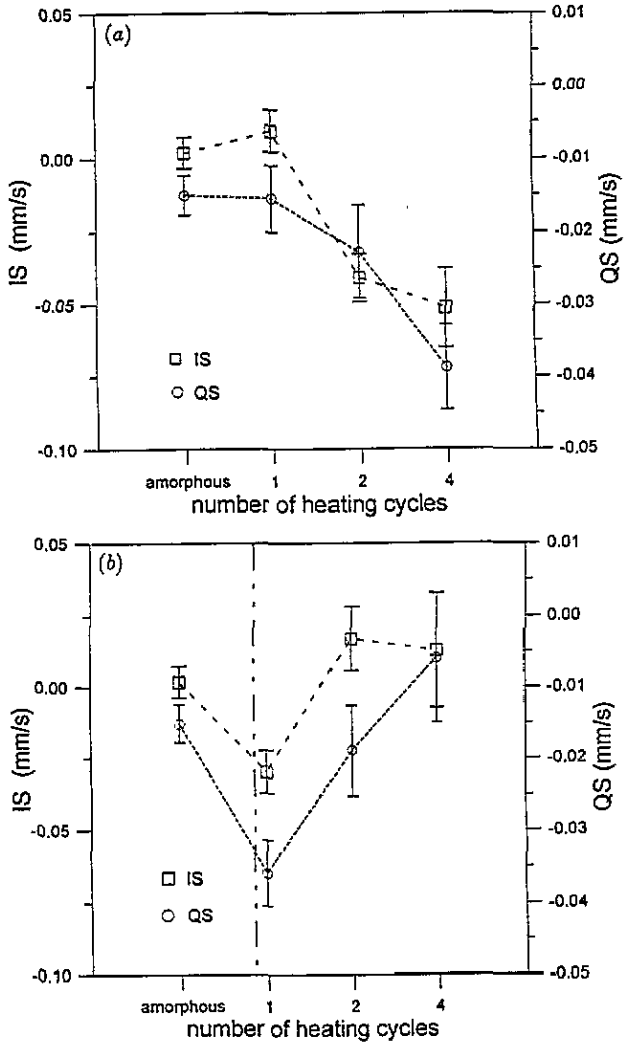

Figure 11. Isomer shift (IS) and quadrupole splitting (QS) evolution as a function of annealing time in the (a) 0MS series and (b) 3MS series.

changes of the amorphous phase which induce formation of nanocrystals and (ii) the main nanocrystallization process. Since both 0MS and 3MS series have amplified the transition between the first stage and the second stage described in the ISO series, the effects of time and temperature are linked in both stages.

3.4. Relaxation of the amorphous phase by annealing at lower temperature

In order to have more insight into the influence of time and temperature in the overall process, two samples isothermally heated for 60 min, at 177 °C and 450 °C, have been analysed. The values obtained for the hyperfine parameters after fitting are shown in table 1. The data quoted there for the 450 °C annealed sample indicate that the first-stage crystallization was already started during annealing at that temperature. Further, a high A23 value (A23 = 3.34) for the amorphous phase is obtained. This means a magnetization mainly parallel to the surface of the ribbon. Therefore, it suggests the existence of an easy axis of magnetization at high temperatures as already reported [7–12].

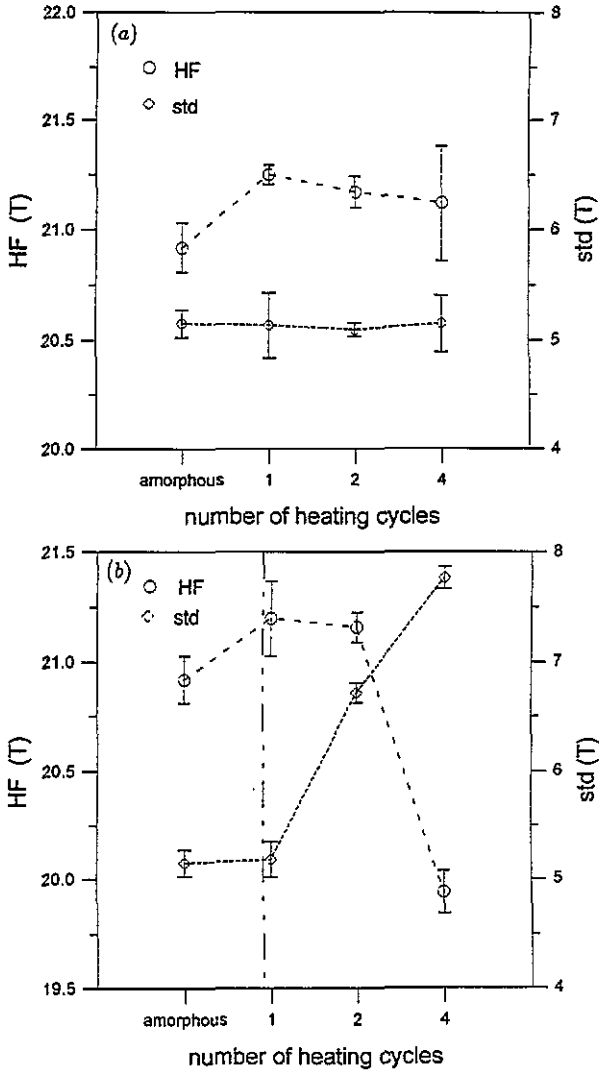

Figure 12. Average magnetic hyperfine-field (HF) and standard deviation (STD) evolution as a function of annealing time in the (a) 0MS series and (b) 3MS series.

In contrast, the fitting parameters of the Mössbauer spectrum of the 177 °C sample show no significant changes compared with those of the amorphous sample, except a slight increase of the A23 value (= 2.26). That is, after such annealing the magnetic moments in the amorphous phase are not randomly distributed. There is an oblate distribution, which may be produced if most of the magnetic moments rotate to become parallel to the surface of the ribbon. This low-temperature relaxation has been obtained for longer annealing (six weeks) at lower temperatures (150 °C) [7, 8, 9].

These results prove that the changes in the distribution of magnetic moment orientations in the amorphous phase are a low-temperature effect (relaxation), which is not related to the onset of crystallization. From isothermal DSC analysis it is found that the first stage of the crystallization process is activated at temperatures of 430 °C, while the second stage appears when annealing above 480 °C. As TEM results indicate that no crystals appear at 177 °C but a few crystalline grains appear at 450 °C with very small sizes ($\langle d \rangle = 5.8$ nm, $\sigma = 2$ nm,

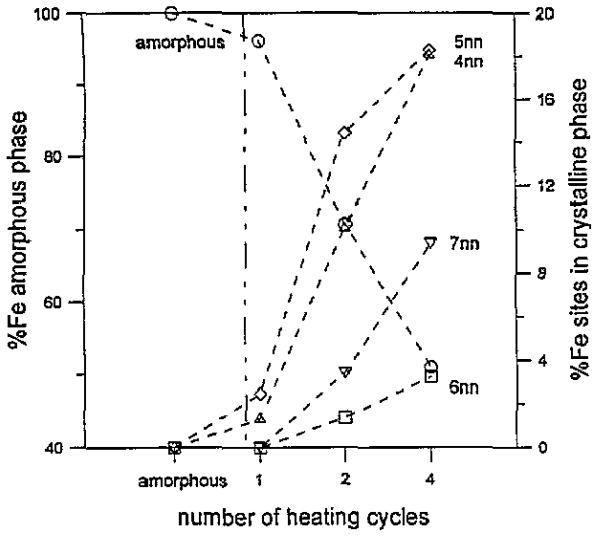

Figure 13. Percentage of iron in the various sites of the nanocrystalline phase as a function of the annealing time in the 3MS series.

and $d_{max} = 8.7$ nm) and low grain density ($N_V = 2.9 \times 10^{15}$ cm^{-3}). Consequently, annealing at about 177 °C, which is below the Curie temperature of the amorphous alloy, brings about an increase of the preferred orientation of the magnetic moments.

Going a step further, raising the annealing temperature, the parameters IS and QS sensitive to short-range order of the amorphous phase decrease. This agrees with a copper diffusion out of the amorphous phase [1, 2, 3], which may be the mechanism responsible of the activation of nanocrystallization. Such a process, called the first stage, occurs prior to a significant appearance of nanocrystalline grains. However, some nanocrystals are already formed in this stage. The second stage appears when annealing or heat treating at a higher temperature (typically above 480 °C), which corresponds to the main nanocrystalline transformation. The grains formed have a DO_3 structure from the very beginning of the nanocrystallization. In the second stage, short-range order changes are detected in the amorphous phase: (i) a decrease in the HF with an increasing width of the magnetic distribution, (ii) an increase in the IS and QS parameters. These changes should be explained as iron diffusion out of the amorphous phase that produces a decrease in the magnetic interaction and a loss of topological and chemical local order around the iron atoms. The evolution of the size distribution and grain density with temperature and annealing time show the characteristic behaviour of a nucleation and growth process.

4. Conclusions

In the $Fe_{73.5}CuNb_3Si_{17.5}B_5$ amorphous alloy two stages of the nanocrystallization process while isothermally annealing at 490 °C have been characterized by Mössbauer spectroscopy. In the first stage the changes of SRO of the amorphous phase are the most important. In the second stage the nanocrystal formation gains in importance. The two stages process of nanocrystallization is probably not restricted to this particular alloy, but extends in a range of FINEMET compositions. Detailed studies on specific alloys is under course.

The first stage lasts only a few minutes after isothermal annealing. It is accompanied by an increase in HF and a decrease in the IS and QS in the amorphous phase. The change of the parameters sensitive to short-range order is interpreted as a change in the local order around the iron atoms. The first-stage crystallization is observed also on 0MS and 3MS series

samples (heating and cooling the amorphous sample from room temperature to 490 °C at a rate of 160 °C m^{-1} several times).

During the second stage the IS and QS of the amorphous phase increase and the HF decreases with an increasing STD. Simultaneously, the relative areas of the various subspectra of the DO_3 phase increase and the absolute iron content in the amorphous phase decreases. The DO_3 phase precipitates in an Si-rich Fe neighbourhood. The silicon content in the nanocrystalline phase decreases from 25 to 22 at.% with increasing annealing time. The grain size distribution measured strongly suggests that nanocrystallization is driven by nucleation and growth.

During the annealing, a tendency of the magnetic moments to orient parallel to the surface of the ribbon is observed (A23 reaches a value of 3.35), especially in the first stage of crystallization. An easy magnetic axis parallel to the surface of ribbon develops at 490 °C. This temperature (490 °C) magnetic orientation has to be differentiated from the low-temperature magnetic relaxation. The low-temperature relaxation was observed when annealing the samples at 177 °C, which is below the Curie temperature of the amorphous alloy. It is shown as an oblate distribution of magnetic moments.

Acknowledgments

The authors wish to thank Dr G Herzer, Vacuumschmelze GmbH, for providing the amorphous ribbons, the Serveis Científico-Tècnics of the Universitat de Barcelona for TEM, Dr J Parellada for the Mössbauer measurement facilities and Dr D Crespo for image analysis. The financial support of the Comisión Interministerial de Ciencia y Tecnología (project No MAT92-0501) is gratefully acknowledged.

References

[1] Yoshizawa Y, Oguma S and Yamauchi K 1988 *J. Appl. Phys.* **64** 6044
[2] Köster U, Schünemann U, Blank-Bewersdorf M, Bauer S, Sutton M and Stephenson G B 1991 *Mater. Sci. Eng.* A **133** 611
[3] Hono K, Hiraga K, Wang Q, Inoue A and Sakurai T 1992 *Surf. Sci.* **266** 385
[4] Herzer G 1993 *Phys. Scr.* **T49** 307
[5] Yoshizawa Y, Yamauchi K 1990 *Mater. Trans. JIM* **31** 307
[6] Noth T H, Lee M B, Kim H J and Kang I K 1990 *J. Appl. Phys.* **67** 5568
[7] Rixecker G, Schaaf P and Gonser U 1992 *J. Phys.: Condens. Matter* **4** 10295
[8] Hampel G, Pundt A and Hesse J 1992 *J. Phys.: Condens. Matter* **4** 3195
[9] Pundt A, Hampel G and Hesse J 1992 *Z. Phys.* **B 87** 65
[10] Miglierini M 1994 *J. Phys.: Condens. Matter* **6** 1431
[11] Kataoka N, Inoue A, Masumoto T, Yoshizawa Y and Yamauchi K 1989 *Japan. J. Appl. Phys.* **28** L1820
[12] Fujinami M, Hashiguchi Y and Yamamoto T 1990 *Japan. J. Appl. Phys.* **29** L477
[13] Clavaguera N, Clavaquera-Mora M T, Zhu J and Beurmann F 1994 *Nanostructured and Non-Crystalline Materials* ed M Vázquez and A Hernando (Singapore: World Scientific) at press
[14] Clavaguera N, Pradell T, Zhu J and Clavaguera-Mora M T 1995 *J. Appl. Phys.* submitted
[15] Brand R A 1990 *NORMOS Programs* version 1990
[16] Hesse J and Rübartsch A 1974 *J. Phys. E: Sci. Instrum* **7** 526
[17] Vandenberghe R E, Gryffroy D and De Grave E 1987 *Nucl. Instrum. Methods Phys. Res.* **B 26** 603
[18] Stearns M B 1963 *Phys. Rev* **129** 1136